Title

Patterned Threadlike Micelles and DNA-Tethered Nanoparticles: A Structural Study of PEGylated Cationic Liposome—DNA Assemblies

Journal

Langmuir, 31(25)

ISSN

0743-7463

Authors

Majzoub, Ramsey N

Ewert, Kai K

Jacovetty, Erica L

et al.

Publication Date

2015-06-30

DOI

10.1021/acs.langmuir.5b00993

HHS Public Access

Author manuscript

Langmuir. Author manuscript; available in PMC 2016 June 30.

Published in final edited form as:

Langmuir. 2015 June 30; 31(25): 7073–7083. doi:10.1021/acs.langmuir.5b00993.

Patterned Thread-like Micelles and DNA-Tethered Nanoparticles: A Structural Study of PEGylated Cationic Liposome–DNA Assemblies

Ramsey N. Majzoub[†], **Kai K. Ewert**[†], **Erica L. Jacovetty**[‡], **Bridget Carragher**[‡,§], **Clinton S. Potter**[‡,§], **Youli Li**[‖], and **Cyrus R. Safinya**[†,*]

[†]Department of Physics, Department of Materials, and Molecular, Cellular and Developmental, Biology Department, University of California, Santa Barbara CA 93106, USA

[‡]National Resource for Automated Molecular Microscopy, Department of Integrative, Structural and Computational Biology, The Scripps Research Institute, 10550 North Torrey Pines Road, La, Jolla, CA 92037, USA

[‖]Materials Research Laboratory, University of California, Santa Barbara CA 93106, USA

Abstract

The self-assembly of oppositely charged biomacromolecules has been extensively studied due to its pertinence in the design of functional nanomaterials. Using cryo electronic microscopy (cryo-EM), optical light scattering and fluorescence microscopy, we investigated the structure and phase behavior of PEGylated (PEG: poly(ethylene-glycol)) cationic liposome–DNA nanoparticles (CL–DNA NPs) as a function of DNA length, topology (linear and circular) and ρ_{chg} (the molar charge ratio of cationic lipid to anionic DNA). Although all NPs studied showed a lamellar internal nanostructure, NPs formed with short (~ 2 kbps), linear, polydisperse DNA were defect-rich and contained smaller domains. Unexpectedly, we found distinctly different equilibrium structures away from the isoelectric point. At $\rho_{chg} > 1$, in the excess cationic lipid regime, thread-like micelles rich in PEG-lipid were found to coexist with NPs, cationic liposomes and spherical micelles. At high concentrations these PEGylated thread-like micelles formed a well-ordered, patterned morphology with highly uniform inter-micellar spacing. At $\rho_{chg} < 1$, in the excess DNA regime and with no added salt, individual NPs were tethered together via long, linear DNA (48 kbps λ-phage DNA) into a biopolymer-mediated floc. Our results provide insight on what equilibrium nanostructures can form when oppositely charged macromolecules self-assemble in aqueous media. Self-assembled, well-ordered thread-like micelles and tethered nanoparticles may have a broad range of applications in bionanotechnology, including nanoscale lithograpy and the development of lipid-based multi-functional nanoparticle networks.

[*]Corresponding Author safinya@mrl.ucsb.edu.

[§]Current Address: National Resource for Automated Molecular Microscopy, New York Structural Biology Center, 89 Convent Avenue, New York, NY 10027 USA

Introduction

Driven by the promise of designable nanomaterials, there is currently very large research activity in the area of self assembly.[1–5] Self-assembly of oppositely charged macromolecules can be used to design nanomaterials with novel optoelectronic[6–8] or environmentally-responsive properties.[9] These nanomaterials have potential applications in biosensing,[10] molecular imprinting,[11] chemical purification,[12] catalysis[13] and drug delivery[4,14] but the principles guiding their design and implementation remain to be fully elucidated. At the molecular length scale, objects interact through a combination of forces,[15] suggesting that a comprehensive understanding of interparticle forces and equilibrium structures is required for self-assembled nanomaterials to achieve their full potential in applications. In systems consisting of oppositely charged macromolecules, a primary driving force for nanomaterials to assemble into well-ordered, stable structures is the entropy gained by the release of counter-ions upon complexation.[16–20] In aqueous media, Poisson-Boltzman theory predicts that highly charged macromolecules are surrounded by a cloud of condensed counter-ions that partially neutralize their charge.[21] When oppositely charged macromolecules approach and neutralize each other, these counter-ions are released into solution, increasing the entropy of the system and minimizing the free energy.[22] While closely related to the electrostatic interaction between oppositely charged entities, this counter-ion release phenomenon enables formation of overcharged structures which are not predicted under simple electrostatics.[18,23] Indeed, nature frequently utilizes counter-ion release for driving the assembly of various biological supra-molecular structures such as the nucleosome.[20,22]

One class of nanomaterials which have applications in biomedicine and are assembled through the counter-ion release mechanism are cationic liposome–DNA (CL–DNA) complexes. [16–18,24–27] CL–DNA complexes are also important systems for investigating self-assembling behavior, and the structure of CL–DNA complexes has been extensively studied using small angle x-ray scattering (SAXS),[16,17] NMR,[28–30] and cryo-EM.[31,32] Complexation of cationic membranes with DNA through counter-ion release shows phase behavior (e.g. lamellar, inverse hexagonal and gyroid cubic phases) that depends on the elastic properties of the membrane (spontaneous curvature, bending modulus, Gaussian modulus) and in some cases nucleic acid length.[4,33–35]

PEGylated CL–DNA complexes have shown more promise as clinically relevant vectors relative to those lacking PEG and have the advantage of increased circulation times in *in vivo* applications.[36,37] Furthermore, the use of a PEG-lipid improves colloidal stability, promotes the spontaneous formation of small, stable nanoparticles (NPs) and provides a platform for covalent attachment of a targeting peptide sequence such as RGD.[38,39] The addition of PEG2K-lipid (PEG MW: 2000 Da) results in unexpected structural features. In the case of CL–DNA complexes, PEGylation alters the internal structure by causing a depletion-attraction force where the intra-particle PEG-lipids phase separate from ordered DNA.[40] Moreover, a recent study has shown that in the case of PEGylated CL–DNA NPs, the number of layers or lamellae per nanoparticle strongly depends on the salt concentration of the assembly buffer because the electrostatic attraction between cationic membranes and anionic DNA (which is weakened by salt screening) must overcome the repulsive steric

force of the grafted polymer.[41] Even outside the context of CL–DNA complexes, studies of liposomal systems show unexpected behavior upon addition of PEG-lipid. For example, in the absence of DNA, PEGylation of liposomes induces the formation of numerous structures which coexist at equilibrium. Alongside liposomes and spherical micelles, long thread-like micelles and bilayer discs have been observed.[42–45]

In this study we used cryo-EM, dynamic light scattering and fluorescence microscopy to investigate the effect of charge ratio (ρ_{chg}: the molar charge ratio of cationic lipids to anionic DNA), DNA length and DNA topology (linear versus circular) on the size, structure and morphology of PEGylated CL–DNA NPs. We found two new phases that appear at ρ_{chg} away from the isoelectric point. Regardless of DNA length or topology, NPs show the lamellar texture (with defects) indicative of the L_{α}^{c} phase with alternating membrane and DNA layers. At $\rho_{chg} > 1$, overall positively charged CL–DNA NPs coexist with spherical liposomes, spherical micelles and thread-like micelles. Interestingly, long thread-like micelles can be induced to form a layered morphology with finger-print like patterns. We show that overall negatively charged PEGylated NPs (at $\rho_{chg} < 1$, in salt-free water with long, linear DNA) form tethered flocs where distinct NPs are bound together with DNA strands that are shared among multiple NPs. Nanoparticles formed via self assembly of oppositely charged macromolecules have a wide range of potential applications and a more detailed picture of their stability and equilibrium structures will aid future design.

Materials and Methods

Materials

The lipids used to prepare the investigated NPs are DOTAP, DOPC and DOPE-PEG2000 (referred to here as PEG2K-lipid), which were purchased as chloroform solutions from Avanti Polar Lipids (Alabaster, AL). For fluorescence experiments liposomes were prepared with 0.2 wt% Texas Red® - 1,2-dihexadecanoyl- *sn*-glycero-3-phosphoethanolamine, triethylammonium salt (Texas Red® DHPE, excitation/emission 595/615 nm) from Invitrogen (Carlsbad, CA). Four distinct types of DNA were used to form nanoparticles; UltraPure Salmon Sperm DNA Solution (S-DNA) (Invitrogen (Carlsbad, CA)), Lambda Phage DNA (λ-DNA) (Thermo Scientific (Waltham, MA)), pGL3 Luciferase Reporter plasmid DNA (pGL3) (Promega (Fitchburg, Wisconsin)), which was propagated via Qiagen Plasmid Plus Mega Kit (Venlo, Limburg) and 11 bp DNA (purchased as single strands from Sigma-Genosys (Sigma-Aldrich (St. Louis, MI) and delivered as a lyophilized film). Complementary single strands were mixed at an equimolar ratio, diluted to a final concentration of 10 mg/mL, heated in a water bath and held at 90 °C for 15 min and slowly cooled to room temperature to allow complete hybridization. For fluorescence studies, DNA was labeled using YOYO-1 (Invitrogen (Carlsbad, CA)) according to the manufacturer's protocol.

Liposome Preparation

Liposomes were prepared by mixing lipids in chloroform solutions at the desired molar ratio in glass vials. The solvent was then evaporated using a stream of nitrogen followed by vacuum dessication for 12 hours. The appropriate amount of high-resistivity (18.2 $M\Omega \cdot m^{-1}$)

water was added to the dry lipid film and incubated at 37 °C overnight. Liposome solutions were then sonicated with a tip sonicator to produce small, unilamellar vesicles.

Cryo Electron Microscopy

The samples were prepared by mixing lipid and DNA solutions at a final concentration of 3 mg/ml or 30 mg/ml, and incubating the CL–DNA solution for 20 minutes. All cryo-EM samples were formed in high-resistivity water except for Fig. 2A and Fig. 3A which were formed at 50 mM NaCl. Next, 3 μL of sample suspension was added to a freshly plasma-cleaned (Solarus plasma cleaner (Gatan Inc. (Pleasanton, CA); 25% O2, 75% Ar mixture) 400-mesh grid Cflat grid, blotted with filter paper for 9 seconds and immediately vitrified in liquid ethane using a Vitrobot (FEI Co. (Hillsboro, OR)). Grids were stored under liquid nitrogen until transfer to the electron microscope for imaging. Vitreous ice grids were transferred into the electron microscope using a cryo-stage that maintains the grids at a temperature of −170 °C. Images were captured using a Tecnai F20 TEM (FEI Co.) operating at 120 keV equipped with a Gatan 4k x 4k CCD camera (Gatan Inc. (Pleasanton, CA)) using the Leginon software system.[46] High magnification images were acquired using a pixel size of 0.22 nm; nominal imaging conditions were an underfocus of ~2.5 μm, and an electron dose of ~20 $e^{-}/Å^{2}$. Fourier transforms and azimuthal integrations were generated using ImageJ.

Dynamic Light Scattering

The size and effective charge measurements of CL–DNA complexes and nanoparticles (NPs) was performed using a Malvern Nanosizer ZS (Malvern Worcestershire, UK). A total of 2 μg of DNA and the appropriate amount of liposome (to achieve the desired lipid/DNA charge ratio) were mixed in 1 mL of the appropriate buffer (high-resistivity water or DMEM as indicated on the figures) and incubated at room temperature for 20 minutes. The solution was then transferred to cuvettes for subsequent measurement. Plots show the z-average diameter D_z which is defined as $D_z = \langle D^6 \rangle / \langle D^5 \rangle$.[47] All zeta potential measurements were performed in high-resistivity water. All data points for dynamic light scattering and zeta potential are the average of two measurements performed on the same sample. Error bars show the standard deviation.

Fluorescence Microscopy

Samples for fluorescence microscopy were prepared using the dyes described in Materials. A total of 50 μL of sample was prepared at the same concentration as for DLS (0.1 μg of DNA and the appropriate amount of lipid based on desired charge ratio), and 2 μl of this solution was placed in between a glass coverslip and slide and sealed with vacuum grease. The solution was imaged with a Nikon Diaphot 300 (Nikon (Tokyo, Japan)) equipped with a Nikon 1.4 NA 60x Plan Apo DIC Objective and Sensicam QE CCD (PCO (Kelheim, German)).

Results and Discussion

DNA Length and Topology Control Internal Nanostructure

The internal structure of PEGylated CL–DNA NPs depends on parameters which include the preferred shape of the constituent lipids (i.e.: related to the spontaneous curvature of the membrane), the membrane bending rigidity and Gaussian modulus.[4] Other parameters which influence phase behavior include PEG-lipid grafting density and ionic strength of the formation buffer.[50] In this work, we investigated the effect of DNA length and topology. Figure 1 shows cropped cryo-EM micrographs (see Figure S1 for whole micrographs) of DOTAP/DOPC/PEG2K-lipid CL–DNA nanoparticles (NPs) formed with linear S-DNA (Salmon Sperm DNA) and Lambda Phage DNA (λ-DNA) and circular pGL3 plasmid (Figure 1 A, B and C respectively). Regardless of DNA length or topology, CL–DNA NPs show a striation pattern indicative of the lamellar phase, which is also seen for CL–DNA complexes without PEG-lipid (Figure S2).

In the case of PEGylated CL–DNA NPs, the number of layers per particle (or domain size) strongly depends on the length and topology of the DNA. S-DNA-based NPs (at 5 mol%) showed fewer layers and more defects (which distorts the layers) than NPs formed from λ-DNA and pGL3. This is despite the fact that the S-DNA-based NPs were formed at a lower grafting density of PEG (5 mol% versus 10 mol%). Previous work[41] found that increasing the PEG-lipid density should result in fewer layers but we found that the length and size distribution of DNA also plays a significant role in determining the number of layers. Moreover, NPs with 5 mol% PEG-lipid should have fewer defects (lamellar defects can be induced by PEG-lipid[49]). Instead we see a more defect rich structure in Fig. 1A due to the use of S-DNA (a highly polydisperse mixture of linear DNA with an average length of 2 kbps). S-DNA-based NPs typically show focal conic defects characteristic of lyotropic lamellar phases.[48] CL–DNA NPs formed with λ-DNA (linear, monodisperse, 48 kbps) show a more coherent layered structure with occasional terminated bilayer edges (Figure 1B, white arrows).

We used a Fourier transform to compare the NP's number of layers as a function of DNA length and polydispersity. Fig. S3 shows images of NPs (approximately ten NPs per image) and a 1D power spectrum measured through azimuthally integrating the Fourier Transform of the images shown in Fig. S3. In the case of λ-DNA and pGL3, the Fourier transform shows a peak due to the lamellar spacing (at $q = 1.07\ nm^{-1}$) where the sharpness of the peak (FWHM) provides a comparative estimate of the number of layers. The S-DNA sample did not show a clear peak due to the low number and distortion of layers.

In the case of pGL3 (Figure 1C), two NPs with distinct morphologies are shown. The first NP (red arrow) has an onion-like structure of alternating layers from the core to the surface. The second NP (dotted white arrow) shows a water filled core surround by a few layers. Similar to NPs containing λ-DNA, NPs formed with pGL3 may also exhibit terminated bilayer edges. Terminated bilayer edges, which are energetically unfavorable due to the exposure of the hydrophobic tails to water, are less frequent in CL–DNA NPs formed with S-DNA. The broad distribution of DNA length in the case of S-DNA could allow rearrangement of the lipid to the most energetically favorable configuration without paying

the energy cost of bending a long piece of DNA. In the case of NPs formed with pGL3 or λ-DNA, the bilayer edges are most likely capped with PEG-lipids which prefer surfaces of high curvature due to their large effective headgroup area.

Thread-Like Cylindrical Micelles at $\rho_{chg} > 1$

Previous work on CL–DNA complexes lacking PEG-lipid has found that increasing ρ_{chg} results in coexistence of CL–DNA complexes and liposomes at equillibirum,[18] but the effect of ρ_{chg} on PEGylated CL–DNA NPs has not received the same attention. Cryo-EM is an ideal technique for investigating lipid- or surfactant-based systems that show populations of distinct structures at equillibirum. [50–54] In Figure 2 we show cryo-EM micrographs of CL–DNA NPs formed at $\rho_{chg} = 3$ (Figure 2A, B) and $\rho_{chg} = 10$ (Figure 2C, G), as well as PEGylated liposomes (Figure 2F, H). The NPs were formed by complexing S-DNA with cationic liposomes at a molar ratio of 80/15/5 DOTAP/DOPC/PEG2K-lipid, while the control samples in Figure 2F contained the same lipid composition but without DNA.

Figure 2A shows that at $\rho_{chg} = 3$, CL–DNA NPs with the lamellar texture (solid arrows) coexist with excess cationic liposomes lacking DNA (dashed arrow) and, unexpectedly, branched thread-like micelles (dotted arrows). In Fig. S4 we present images and corresponding statistical results for counting the number of CL–DNA NPs and cationic liposomes. At ρ_{chg} =3 and 80/15/5 DOTAP/DOPC/ PEG2K-lipid with S-DNA, the NP to cationic lipid ratio is approximately 1:1.3. We expect this ratio to strongly depend on ρ_{chg}.

The sample in Figure 2A was extensively centrifuged (15 min at 4,000 *g*) to form a pellet of CL–DNA NPs and resuspended before addition to the cryo-EM grid for vitrification and subsequent imaging. Previous work[16,17,40] has shown that centrifugation, which is frequently used to prepare samples for small angle x-ray scattering, drives CL–DNA complexes towards equilibrium more quickly. Interestingly, although the sample was subjected to centrifugation, the NPs remain as distinct individual objects due to the presence of the PEG brush layer which sterically stabilizes the NPs. This is in contrast to CL–DNA complexes lacking PEG-lipid, which form large, aggregates with sizes above one micrometer (Supplementary Figure S2).

Another interesting feature in Figure 2A is the deformation of the larger liposomes (yellow dashed arrow). When a cryo-EM sample is dehydrated through blotting, an effective osmotic pressure is applied to the sample. The sample could respond to this pressure through reduced inter-particle spacings but instead, due to the steric repulsion of PEG-lipids, larger liposomes deform suggesting the sample is under osmotic pressure due to packing of NPs via blotting.

Figure 2B,C show micrographs of CL–DNA NPs formed at charge ratios of $\rho_{chg} = 3$ and $\rho_{chg} = 10$ respectively, but now at very low concentrations. In Figure 2C,G similar to what was observed in Figure 1A, NPs (solid arrows), liposomes (dashed arrows) and both spherical and elongated micelles (dotted arrows) coexist. In contrast to Figure 2A, due to the low concentration, NPs are found near the edges of the carbon hole, where a thicker water layer allows liposomes to remain spherical. This suggests that at low concentrations of materials, no blotting-induced osmotic pressure deforms the liposomes.

Control samples consisting of cationic liposome preparations with no added DNA (Figure 2D, H) show spherical liposomes (solid arrow) and spherical micelles (dotted arrow), but surprisingly none of the cylindrical micelles found in preparations of CL–DNA NPs (dotted arrows (Figure 2A)). We will return to a detailed discussion of cylindrical micelles when discussing Figure 3.

Figure 2E shows the zeta potential as a function of ρ_{chg} for NPs of varying mol% PEG2K-lipid. The zeta potential is measured by detecting the velocity of charged NPs under the influence of an electric field in solution. Using force balance, the electrostatic potential at a hypothetical slipping plane can be measured by assuming that the charges within the plane move in concert with the NP.[55] As a function of ρ_{chg}, the zeta potential increases from with ρ_{chg} from approximately −30 mV for ρ_{chg} = 1/3, crossing 0 mV just above ρ_{chg} = 1 and saturating at around +50 mV at ρ_{chg} =5 and 10. AS reported for CL–DNA complexes lacking PEG-lipid (both in experiments [18] and theoretical work[23]), when increasing ρ_{chg} above the isoelectric point the complexes or NPs incorporate excess lipid and the zeta potential increases until it becomes energetically more favorable for the NPs to expel excess cationic liposomes and the zeta potential saturates. For ρ_{chg} < 1, below the isoelectric point, the NPs are negatively overcharged (i.e., they containing more DNA within the NP than required to neutralize the cationic lipids) and coexist with excess DNA in solution (further discussed with Figure 5). As the extent of PEGylation (molar fraction of PEG-lipid) increases, the surface-grafted PEG pushes the slipping plane away from the NP, reducing the zeta potential.[38]

Figure 2F shows the zeta potential as a function of mol% cationic lipid for NPs at ρ_{chg} = 1/3 and ρ_{chg} = 10. The maximum level of overcharging (both positive and negative) achievable by NPs increases with mol% cationic lipid. For overcharged cationic CL–DNA NPs, solving the linearized Poisson-Boltzman equation shows that the electrostatic potential, $\phi(x)$, scales linearly with membrane charge density: $\varphi(x)=\frac{\sigma}{\varepsilon_r\varepsilon_0\kappa}e^{-\kappa x}$, where σ is the membrane charge density, ε_r and ε_0 are the dielectric constant of water and permittivity of free space respectively, and κ is the inverse Debye length.[23] This membrane charge density is directly proportional to mol% cationic lipid, and the zeta potential increase with mol% cationic lipid at high ρ_{chg} is thus expected. The maximal anionic zeta potential increasing with mol% cationic lipid is not intuitive within the context of Possion-Boltzman theory. In fact, previous literature reports that investigated the overcharging phenomena in CL–DNA complexes lacking PEG2K-lipid found that complexes with higher DOPC (neutral lipid) content (lower membrane charge density) could incorporate more anionic DNA due to reduced DNA-DNA repulsion in complexes with more neutral lipids and thus larger DNA spacings. [16,18], One possible explanation for the increase in maximum anionic zeta potential with mol fraction cationic lipid is that the size of NPs increases with addition of neutral lipid (see Fig. S5) which increases the radius of the slipping plane, *R*, at a given charge *Q* ($\zeta \propto Q/R$, where the charge *Q* depends on ρ_{chg}).

Figure 2A showed small thread-like micelles coexisting with liposomes and CL–DNA NPs. Figure 3A shows another carbon hole from the same EM grid, where sample preparation has spatially organized the NPs, liposomes and micelles according to their size. In the center of

the hole are long thread-like micelles, which have formed a finger print-like pattern with regular inter-micelle spacing; closer to the edge, liposomes and NPs are visible. Thread-like micelles containing PEG2K-lipid in the absence of DNA have been previously reported in the literature[42–44] but to our knowledge have never been observed in CL–DNA samples. The thread-like (or cylindrical) micelles are preferentially found in the center of the carbon hole where the suspended solution film is at its thinnest. This suggests that the well-ordered packing of the micelles is caused by sample preparation, where an effective osmotic pressure is applied to the concentrated PEGylated CL–DNA NPs through the removal of water during blotting. We expect that the ordering of thread-like micelles may also be obtained by the addition of osmotic stress-inducing agents (e.g., a high concentration of free PEG with size larger than the inter-micellar spacing), which would remove water in a controlled manner.

Figure 3B shows the Fourier transform of the boxed region in Figure 3A. In the Fourier transform, we note two clearly visible rings resulting from the first and second harmonic of the structure factor of uniformly spaced micelles. A 1D radial scan of the Fourier transform (integrated over all angles in the 2D plane) is shown in Figure 3C. The two structure factor peaks at $q_{01} = 0.4394\ nm^{-1}$ and $q_{02} = 0.8850\ nm^{-1}$ correspond to the inter-micelle spacing of $d = (2\pi/q_{01}) = 14.25 \pm 0.05$ nm. The structure factor of the well-ordered micelles is multiplied by the form factor of the cylindrical micelles. The q value for a form factor minimum (q_m) corresponds to an effective object size (micelle diameter) in real space of $\delta_m = 2\pi/q_m = 3.727$ nm. This thickness is in excellent agreement with previous measurements[19] of lipid bilayers formed with similar compositions. Subtracting the thickness of the micelle from the micelle spacing we get an inter-micelle water layer thickness of $\delta_w = 10.52$ nm. Assuming that the water layer contains two grafted PEG2K molecules, we can estimate the thickness of each PEG molecule as $L = \delta_w/2 = 5.26$ nm. This thickness is low compared to what has been measured for grafted PEG2K using small angle x-ray scattering[56] and surface force apparatus[57] (SFA) ($L = 6.6$ nm and $6.5\ nm < L < 7.5$ nm for SAXS and SFA, respectively). This discrepancy could be due to the blotting-induced pressure applied to the sample. Similar thread-like micelles have been reported in lipid-only (no DNA) systems containing DOPC or Egg-PC with DSPE-PEG2000[42–45] (in contrast to our DOPE-PEG2000), but to our knowledge this is the first time PEGylated thread-like micelles have been shown to order over large length scales (the diameter of the carbon hole is 2 μm). It has been previously reported[53] that the thickness of a water film suspended in a carbon hole can range between 10 – 500 nm. The fact that the center of the carbon hole only shows one stack of two dimensionally packed thread-like micelles implies that the ice thickness in this region is less than 30 nm (the approximate thickness of two micelles). However, certain regions in Fig. 3A do contain multiple stacks of thread-like micelles (orange arrows).

Similar to our results, Sandstrom et al. found coexistence of multiple micelle phases for a given sample composition.[45] Previous work in liposome/micelle phase behavior focused on two-component systems (typically a neutral lipid and a PEG-lipid) and did not find thread-like micelles until the mol% of PEG-lipid went beyond 20 mol%. This suggests that thread-like micelle formation occurs when the grafting density of PEG chains is large enough that the average spacing between PEG-lipids becomes less than twice the radius of gyration (i.e.

near the mushroom-brush transition). Thus, unfavorable packing of grafted PEG polymers leads to phase separation where fully covered liposomes coexist with micelles.

What is interesting about our study compared to previous work,[42,43] is that thread-like micelles appear at much lower grafting densities (5 mol% DOPE-PEG2K vs. 25 mol% DSPE-PEG2K). This strongly suggests that complexation of DNA with PEGylated cationic liposomes results in partial expulsion of the excess PEG2K-lipid into spherical and cylindrical micelles. The existence of cylindrical micelles, which previous reports only observe in the case of neutral lipid/PEG-lipid dispersions, implies that non-PEGylated lipid is also being expelled from the CL-DNA NPs. PEG-lipids have large effective headgroup areas due to the steric repulsion of PEG and will favor surfaces with positive spontaneous curvature (e.g., spherical micelles). A cylindrical micelle has positive curvature in one direction and zero curvature along the micelle, suggesting that the cylindrical micelles not only contain PEG-lipid but also cationic and/or neutral lipids, which prefer surfaces of zero curvature.

A simple argument based on geometry can explain why complexation with DNA will expel PEG2K-lipid. At the mol fraction of cationic lipid used in the sample shown in Figure 2 and Figure 3 (80/15/5 DOTAP/DOPC/PEG2K-lipid), SAXS measurements have shown that the DNA-DNA spacing is on the order of the diameter of hydrated DNA.[18] This means that the PEG2K-lipid and DNA will compete for the limited available space between cationic membranes> The added crowding due to the presence of DNA (which is electrostatically bound to the membranes) favors phase separation and PEGylated micelle formation, which thus occurs at lower mol% compared to neutral lipid/PEG-lipid dispersions. Figure 4 contains a schematic which summarizes our model for the formation of thread-like micelles based on previous work done on PEGylated CL–DNA NPs. The observation that micelles form suggests that the free energy gain through counter-ion release (i.e., the driving force for the intercalation of DNA between cationic membranes) is larger than the loss of entropy incurred from multi-phase coexistence.

Interestingly, previous SAXS reports[40,41] on CL–DNA NPs did not see indications of micelle formation in the scattering data. We believe that due to the electron dense-nature of CL–DNA NPs, their q_{01} and q_{DNA} peaks dominate the scattering signal. Furthermore, previous x-ray work was performed without inducing osmotic pressure suggesting that the carbon hole imaged in Figure 2A (which contains a thicker water film as evident from the larger NPs found near the center of the hole) is a more accurate representation of the x-ray pellets. In this case (Figure 2A), the thread-like micelles were dispersed among liposomes and CL–DNA NPs as opposed to spatially segregated into a well-ordered pattern. When thread-like micelles are prepared without DNA (using high concentrations of PEG-lipid), previous work[44] has shown that they can be detected with either SAXS and SANS. These well-ordered, thread-like micelles could have applications as masks in nanoscale lithography

DNA-induced Tethering of NPs

We used dynamic light scattering (DLS) to measure the hydrodynamic diameter of our NPs in the dilute regime. Previous work has shown that statistically meaningful size measurements can be extracted from cryo-EM micrographs[58] but the high-throughput nature

of DLS allowed us to investigate size as a function of DNA length, PEG2K grafting density, buffer ionic strength and ρ_{chg}. In particular, the z-average hydrodynamic diameter measured through DLS provides statistically meaningful trends in size.[47]

Figure 5A–D shows the hydrodynamic diameter of NPs as a function of the charge ratio (ρ_{chg}) for circular (pGL3), polydisperse (S-DNA), short (11 bp) and long (λ-DNA) DNA in high-resistivity water and DMEM. In the case of pGL3, S-DNA and 11 bp DNA, a maximum in size is evident near the calculated isolectric point $\rho_{chg} = 1$) of the NPs. This is expected because the size of NPs is a result of competing electrostatic self-energy (which favors smaller particles) and surface tension (which favors large particles that minimize the surface area to volume). At the isoelectric point, NPs are near charge-neutral, reducing the electrostatic self-energy and causing individual NPs to form at larger sizes. In comparison to isoelectric CL–DNA complexes without PEG-lipid, isoelectric PEGylated CL-DNA NPs are smaller by an order of magnitude (≈ 200 nm versus > 1 μm). We attribute this to the steric repulsion of the PEG brushes, which coat the NPs and prevent aggregation due to van der Waals attraction. Interestingly, NPs formed with λ-DNA (Fig. 5D) do not show a maximum in size near the isoelectric point but instead continue to grow as the charge ratio decreases beyond the isoelectric point ($\rho_{chg} < 1$). This observation will be further investigated using cyro-EM and fluorescence microscopy in a later section.

When formed in DMEM, the NP's size shows DNA-dependence, where NPs composed of λ-DNA are the on average larger than NPs formed with S-DNA, pGL3 or 11 bp DNA. This can be understood by considering that the length of λ-DNA sets a minimum NP size which alters the size distribution of NPs. To calculate the minimum NP size due to the volume of DNA, we can compare the surface area of λ- DNA to total available bilayer area. In the case of λ-DNA, the surface area (A_{DNA}) is $A_{DNA} = w \times L_{bp} \times N_{bp}$ where w is the diameter of hydrated DNA (25 Å), L_{bp} is the distance between base pairs (3.3 Å) and N_{BP} is the number of base pairs or nucleotides (48,502 in the case of λ-DNA). For an onion-like particle of diameter D and layer spacing d, the total lipid surface area (A_L) in the particle can be approximated by dividing the volume of the sphere by the layer spacing (d): $A_L = ((4/3)\pi(D/;2)^3)/d$. Setting A_{DNA} equal to A_L and solving for the diameter, in the case of λ-DNA the minimum nanoparticle diameter is D_{min} = 78 nm. This suggests that the sizes of NPs formed with S-DNA, pGL3 or 11 bp DNA are the result of the competing electrostatic and surface tension forces described earlier while NPs formed with λ-DNA contain size truncated size distributions due to the DNA's size.

Figure 5E,F shows the dependence of the NP's size on salt concentration. Regardless of DNA type or the NP's molar charge ratio, the average particle size decreases as salt concentration increases. This is evident from Figure 5A–D: NPs formed in water are typically larger than NPs formed in the biological buffer DMEM (≈ 150 mM 1:1 salt and ≈ 3 mM 2:1 salt). This is an interesting result because PEGylated CL–DNA NPs show completely different salt concentration dependent behavior from non-PEGylated CL–DNA complexes. Addition of salt decreases the Debye screening length and thereby reduces the electrostatic repulsion between two like-charged CL–DNA complexes, thus causing them to aggregate and increasing their effective size. In the case of PEGylated CL–DNA NPs, complexation of PEGylated liposomes and DNA in the presence of increasingly higher

concentrations of salt, up to the physiological regime (≈ 200 mM 1:1 salt) has been shown to form NPs with correspondingly fewer layers.[41] This is because increasing salt concentration reduces the attractive electrostatic force between cationic membrane and DNA, impeding the DNA's ability to overcome the PEG-induced steric force and undergo complexation with the cationic membrane. Thus, the size of the NPs decreases with increasing ionic strength.

Figure 5G shows the average size of PEGylated liposomes as a function of mol% PEG2K-lipid. Initially, the addition of PEG2K-lipid reduces the average size of liposomes, most likely by preventing fusion of liposomes, but as PEG2K-lipid mol% increases beyond 5 mol % the size of the liposomes slightly increases. CL-DNA NPs (Fig. 5A, B, D) were found to be larger than cationic liposomes without DNA (Fig. 4G) except in the case of CL-DNA NPs formed with 11 bp DNA (Fig. 5C).

The most interesting feature in the DLS data is the observation that NPs based on λ-DNA (Figure 5D) do not show a maximum in size near the isolectric point but instead continue to grow as the charge ratio approaches zero ($\rho_{chg} < 1$). To gain greater insight into this observation we imaged our NPs using fluorescence and differential interference contrast (DIC) microscopy. Fig. 6A displays DIC and fluorescent images of NPs which have been dual-labeled using Texas Red-DHPE (lipid channel) and Yoyo-1 (DNA channel). The images show NPs formed with either λ-DNA or pGL3 at $\rho_{chg} = 1/3$ (excess DNA regime) or $\rho_{chg} = 3$ (excess cationic lipid regime) in high-resistivity water or 150 mM NaCl. NPs with $\rho_{chg} = 3$ show excess liposomes that lack DNA (fluorescent spots in lipid channel with no corresponding spot in DNA channel), as was observed in the cryo-EM micrographs (Fig. 2A). A comparison between DNA fluorescent channels is quite revealing. All cases show fluorescent spots with some variations in size. However, for λ-DNA at $\rho_{chg} = 1/3$ formed in water, a fuzzy DNA cloud surrounds the DNA spots (i.e., regions of condensed DNA), which colocalize with lipid solid arrow in lipid channel and corresponding condensed DNA in DNA channel). Long λ-DNA in salt-free buffer acts as a tether or bridge between negatively overcharged NPs, giving rise to the observed fuzzy cloud in the excess DNA regime at $\rho_{chg} < 1$. The tethering of NPs may be expected to result in a higher likelihood of collisions between NPs and fusion leading to the increased size of λ-DNA NPs at $\rho_{chg} < 1$ observed in DLS (Figure 5D).

Figure 6B,C shows cyro-EM images of NPs formed with 80/15/5 DOTAP/DOPC/ PEG2K-lipid and S-DNA at $\rho_{chg} = 1/3$ (Figure 6B) and $\rho_{chg} = 3$ (Figure 6C). Figure 6B shows that NPs formed at $\rho_{chg} < 1$ coexist with excess DNA (asterisk) at equilibrium. In contrast, Figure 6C (CL–DNA NP at $\rho_{chg} = 3$) shows no excess DNA in the background. The NP in Figure 6B illustrates the morphology of tethered NPs. An onion-like NP (solid white arrow) is tethered to two smaller NPs (dashed white arrows) where one of them is in very close contact with a third NP (black dashed arrow) which has partially fused.

Figure 6D,E displays two micrographs from a sample composed of NPs with 80/10/10 DOTAP/DOPC/PEG2K-lipid and 11 bp DNA at $\rho_{chg} = 1/3$. Figure 6D shows NPs with two distinct morphologies. The red arrow highlights an onion-like NP containing nearly perfect concentric layers. The yellow arrow highlights a featureless electron-dense globular NP.

Similar electron-dense structures have been previously reported when NPs containing siRNA are formed with microfluidic mixing.[59] Although this previous report determined the structure of their electron-dense nanoparticles, the featureless morphology we observe in our cryo-EM micrographs suggests an unstructured core. Surprisingly, it seems that mixtures of short 11 bp DNA with PEGylated cationic liposomes can spontaneously self-assemble into this structure at $\rho_{chg} < 1$. There is no evidence of tethering in the case of NPs formed with 11 bp DNA.

Figure 6E shows a micrograph of the excess 11 bp DNA that coexists with NPs at $\rho_{chg} = 1/3$. As expected, short 11 bp DNA molecules appear as small black spots instead of long, ordered polymers (asterisk in Figure 5B). In agreement with previous work,[60] the concentration of 11 bp DNA imaged in Figure 6E is too low to see liquid crystal phases, but there is in fact evidence of 11 bp DNA stacking (white arrow).

Conclusion

In this paper (combining cryo-EM, fluorescence microscopy, and DLS) we have presented a comprehensive study of structures formed with PEGylated CL–DNA NPs, covering the regimes of excess cationic lipid ($\rho_{chg} > 1$) and excess DNA ($\rho_{chg} < 1$). The internal lamellar nanostructure of the NPs depends on the DNA: short, linear polydisperse DNA resulted in smaller domains and defect-rich NPs. Varying ρ_{chg}, we found unexpected new structures including thread-like micelles coexisting with NPs in the excess cationic membrane regime ($\rho_{chg} > 1$) and DNA-tethered NPs in the excess DNA regime ($\rho_{chg} < 1$). Our cryo-EM results highlight the importance of imaging samples that contain a heterogeneous mixture of structures at equilibrium. Because of the CL–DNA NPs' comparatively high difference in electron density and index of refraction from the medium, the signal from CL–DNA NPs will dominate in SAXS and DLS. This makes coexisting liposomes or micelles hard to detect.

These new structures should aid in the design of functional bionanotechnological materials that form through self-assembly of oppositely charged macromolecules in aqueous media. The 1D ordered thread-like (or cylindrical) micelles with controllable nanometer-scale inter-micellar spacing may have applications in nanolithography. The new phase of tethered CL–DNA NPs could have applications in nucleic acid delivery and beyond. For gene delivery, the tethered phase could be a means for delivering large genes without the need for forming large particles. The individual NPs within the tether could reorganize, allowing the flocs to penetrate small capillaries or endothelial clefts. The tethered phase could also be useful in applications that require multiple nanoparticles with distinct functions to remain spatially localized relative to one another.

Supplementary Material

Refer to Web version on PubMed Central for supplementary material.

Acknowledgements

This research was primarily supported by the U.S. Department of Energy (DOE), Office of Science, Basic Energy Sciences (BES), under award DE–FG02–06ER46314 (electrostatic assembly of charged membranes with DNA with distinct length and geometry), the National Science Foundation (NSF) under award DMR-1401784 (phase behavior of bio-nanoparticles), and the National Institute of Health (assembly of nanoparticles with short DNA as models of siRNA) under award GM-59288. The DLS Measurements made use of the Central Facilities of the Materials Research Laboratory at UCSB which is supported by the MRSEC Program of the NSF under award no. DMR-1121053. The EM work was conducted at the National Resource for Automated Molecular Microscopy at The Scripps Research Institute, which is supported by the NIH Biomedical Technology Research Resources program (GM103310) of the National Institute of General Medical Sciences (BC, CSP).

References

1. Kim T-H, Kang S-H, Doe C, Yu J, Sim J-B, Kim J, Kline SR, Choi S-M. Highly Ordered Self-Assembly of 1D Nanoparticles in Phospholipids Driven by Curvature and Electrostatic Interaction. J. Amer. Chem Soc. 2009; 131:7456–7460. [PubMed: 19469580]
2. Grzelczak M, Vermant J, Furst EM, Liz-Marzan LM. Directed Self-Assembly of Nanoparticles. ACS Nano. 2010; 4:3591–3605. [PubMed: 20568710]
3. Hamley IW. Self-assembly of Amphiphilic Peptides. Soft Matter. 2011; 7:4122–4138.
4. Safinya CR, Ewert KK, Majzoub RN, Leal C. Cationic Liposome-Nucleic Acid Complexes for Gene Delivery and Gene Silencing. New J. Chem. 2014; 38:5164–5172.
5. Stupp SI, Zha RH, Palmer LC, Cui H, Bitton R. Self-Assembly of Biomolecular Soft Matter. Faraday Discuss. 2013; 166:9–30. [PubMed: 24611266]
6. Mirkin CA, Letsinger RL, Mucic RC, Storhoff JJ. A DNA-based Method for Rationally Assembling Nanoparticles into Macroscopic Materials. Nature. 1996; 382:607–609. [PubMed: 8757129]
7. Hu J, Li L, Yang W, Manna L, Wang L, Alivisatos AP. Linearly Polarized Emission from Colloidal Semiconductor Quantum Rods. Science. 2001; 292:2060–2063. [PubMed: 11337589]
8. Lee M, Im J, Lee BY, Myung S, Kang J, Huang L, Kwon Y-K, Hong S. Linker-free Directed Assembly of High-Performance Integrated Devices Based on Nanotubes and Nanowires. Nature Nanotech. 2006; 1:66–71.
9. Shirazi RS, Ewert KK, Leal C, Majzoub RN, Bouxsein NF, Safinya CR. Synthesis and Characterization of Degradable Multivalent Cationic Lipids with Disulfide-bond Spacers for Gene Delivery. Biochim. Biophys. Acta - Biomembranes. 2011; 1808:2156–2166.
10. Arya SK, Solanki PR, Datta M, Malhotra BD. Recent Advances in Self-Assembled Monolayers based Biomolecular Electronic Devices. Biosens. and Bioelect. 2009; 24:2810–2817.
11. Liang H, Angelini TE, Ho J, Braun PV, Wong GCL. Molecular Imprinting of Biomineralized CdS Nanostructures: Crystallographic Control using Self-Assembled DNA-Membrane Templates. J. Amer. Chem. Soc. 2009; 125:11786–11787. [PubMed: 14505378]
12. Turek VA, Elliot LN, Tyler AII, Demetriadou A, Paget J, Cecchini MP, Kucernak AR, Kornyshev AA, Edel JB. Self-assembly and Applications of Ultraconcentrated Nanoparticle Solutions. ACS Nano. 2013; 7:8753–8759. [PubMed: 24070428]
13. Wang Z-G, Zhan P, Ding B. Self-assembled Catalytic DNA Nanostructures for Synthesis of Para-directed Polyaniline. ACS Nano. 2013; 7:1591–1598. [PubMed: 23272944]
14. Chan C-L, Majzoub RN, Shirazi RS, Ewert KK, Chen Y-J, Liang KS, Safinya CR. Endosomal Escape and Transfection Efficiency of PEGylated Cationic Liposome-DNA Complexes Prepared with an Acid-Labile PEG-Lipid. Biomaterials. 2012; 33:4928–4935. [PubMed: 22469293]
15. Israelchvili, J. Intermolecular and surface forces, Third Edition: Revised Third Edition. Burlington: Elsevier; 2011.
16. Radler JO, Koltover I, Salditt T, Safinya CR. Structure of DNA-Cationic Liposome Complexes: DNA Intercalation in Multilamellar Membranes in Distinct Interhelical Packing Regimes. Science. 1997; 275:810–814. [PubMed: 9012343]
17. Koltover I, Salditt T, Radler JO, Safinya CR. An Inverted Hexagonal Phase of Cationic Liposome-DNA Complexes Related to DNA Release and Delivery. Science. 1998; 281:78–81. [PubMed: 9651248]

18. Koltover I, Salditt T, Safinya CR. Phase diagram, Stability and Overcharging of Lamellar Cationic Lipid-DNA Self-assembled Complexes. Biophys. J. 1999; 77:915–924. [PubMed: 10423436]
19. Dehaseth PL, Lohman TM, Record MT. Interpretation of Monovalent and Divalent Cation Effects on the lac Repressor-Operator Interaction. Biochemistry. 1977; 16:4791–4796. [PubMed: 911790]
20. Gelbart WM, Bruinsma RF, Pincus PA, Parsegian VA. DNA Inspired Electrostatics. Physics Today. 2000; 53:38–44.
21. Manning G. Limiting Laws and Counterion Condensation in Polyelectrolyte Solutions I Colligative Properties. J. Chem. Phys. 1969; 51:924–933.
22. Harries D, May S, Ben-Shaul A. Counterion Release in Membrane-Biopolymer Interactions. Soft Matter. 2013; 9:9268–9284.
23. Bruinsma R. Electrostatics of DNA-cationic lipid complexes: isoelectric instability. Eur. Phys. J. 1998; 4:75–88.
24. Felgner PL, Gadek TR, Holm M, Roman R, Chan HW, Wenz M, Northrop JP, Ringold GM, Danielsen M. Lipofection: A Highly Efficient, Lipid-Mediated DNA-Transfection Procedure. Proc. Natl. Acad. Sci. U.S.A. 1987; 84:7413–7417. [PubMed: 2823261]
25. Yin H, Kanasty RL, Eltoukhy AA, Vegas AJ, Dorkin JR, Anderson DG. Non-viral Vectors for Gene-Based Therapy. Nat. Rev. Genet. 2014; 15:541–555. [PubMed: 25022906]
26. Guo X, Huang L. Recent Advances in Nonviral Vectors for Gene Delivery. Acc. Chem. Res. 2012; 45:971–979. [PubMed: 21870813]
27. Chan C-L, Ewert KK, Majzoub RN, Hwu Y-K, Liang KS, Leal C, Safinya CR. Optimizing Cationic and Neutral Lipids for Efficient Gene Delivery at High Serum Content. J. Gene Med. 2014; 16:84–96. [PubMed: 24753287]
28. Mok KW, Cullis PR. Structural and Fusogenic Properties of Cationic Liposomes in the Presence of Plasmid DNA. Biophys. J. 1997; 73:2534–2545. [PubMed: 9370447]
29. Leal C, Topgaard D, Martin RW, Wennerstrom H. NMR Studies of Molecular Mobility in DNA-Amphiphile Complex. J. Phys. Chem. 2004; 108:15392–15397.
30. Leal C, Sandstrom D, Nevsten P, Topgaard D. Local and translational dynamics in DNA-lipid Assemblies Monitored by Solid-State and Diffusion NMR. Biochim. Biophys. Acta - Biomembranes. 2008; 1778:214–228.
31. Battersby BJ, Grimm R, Huebner S, Cevc G. Evidence for Three-Dimensional Interlayer Correlations in Cationic Lipid-DNA Complexes as Observed by Cryo-Electron Microscopy. Biochim. Biophys. Acta - Biomembranes. 1998; 1372:379–383.
32. Huebner S, Battersby BJ, Grimm R, Cevc G. Lipid-DNA Complex Formation: Reorganization and Rupture of Lipid Vesicles in the Presence of DNA as Observed by Cryoelectron Microscopy. Biophys. J. 1999; 76:3158–3166. [PubMed: 10354440]
33. Leal C, Bouxsein NF, Ewert KK, Safinya CR. Highly Efficient Gene Silencing Activity of siRNA Embedded in a Nanostructured Gyroid Cubic Lipid Matrix. J. Amer. Chem. Soc. 2010; 132:16841–16847. [PubMed: 21028803]
34. Bouxsein NF, Leal C, McAllister CS, Ewert KK, Li Y, Samuel CE, Safinya CR. Two-Dimensional Packing of Short DNA with Nonpairing Overhangs in Cationic Liposome-DNA Complexes: From Onsager Nematics to Columnar Nematics. J. Am. Chem. Soc. 2011; 133:7585–7595. [PubMed: 21520947]
35. May S, Harries D, Ben-Shaul A. The Phase Behavior of Cationic Lipid-DNA Complexes. Biophys. J. 2000; 78:1681–1697. [PubMed: 10733951]
36. Immordino ML, Dosio F, Cattel L. Stealth Liposomes: Review of the Basic Science, Rationale and Clinical Applications, Existing and Potential. Int. J. Nanomedicine. 2006; 1:297–315. [PubMed: 17717971]
37. Morille M, Montier T, Legras P, Carmoy C, Brodin P, Pittard B, Benoit J-P, Passirani C. Long-circulating DNA Lipid Nanocapsules as New Vector for Passive Tumor Targeting. Biomaterials. 2010; 31:321–329. [PubMed: 19800113]
38. Majzoub RN, Chan C-L, Ewert KK, Silva BFB, Liang KS, Jacovetty EL, Carragher B, Potter CS, Safinya CR. Uptake and Transfection Efficiency of PEGylated Cationic Liposome-DNA Complexes with and without RGD-Tagging. Biomaterials. 2014; 35:4996–5005. [PubMed: 24661552]

39. Majzoub RN, Chan C-L, Ewert KK, Silva BFB, Liang KS, Safinya CR. Fluorescence microscopy colocalization of lipid-nucleic acid nanoparticles with wildtype and mutant Rab5-GFP: A platform for investigating early endosomal events. Biochim. Biophys. Acta – Biomembranes. 2015 accepted.
40. Martin-Herranz A, Ahmad A, Evans HM, Ewert KK, Schulze U, Safinya CR. Surface Functionalized Cationic Lipid-DNA Complexes for Gene Delivery: PEGylated Lamellar Complexes Exhibit Distinct DNA-DNA Interaction Regimes. Biophys. J. 2004; 86:1160–1168. [PubMed: 14747350]
41. Silva BFB, Majzoub RN, Chan C-L, Li Y, Olsson U, Safinya CR. Pegylated Cationic Liposome-DNA Complexation in Brine is Pathway-Dependent. Biochim. Biophys. Acta - Biomembranes. 2014; 1838:398–412.
42. Johansoon E, Sandstrom MC, Bergstrom M, Edwards K. On the Formation of Discoidal versus Threadlike Micelles in Dilute Aqueous Surfactant/Lipid Systems. Langmuir. 2008; 24:1731–1739. [PubMed: 18215080]
43. Johnson M, Edwards K. Liposomes, Disks, and Spherical Micelles: Aggregate Structure in Mixtures of Gel Phase Phosphatidylcholines and Poly(Ethylene Glycol)-Phospholipids. Biophys. J. 2003; 85:3839–3847. [PubMed: 14645073]
44. Arleth L, Ashok B, Onyuksel H, Thiyagarajan P, Jacob J, Hjelm RP. Detailed Structure of Hairy Mixed Micelles Formed by Phosphatidylcholine and PEGylated Phospholipids in Aqueous Media. Langmuir. 2005; 21:3279–3290. [PubMed: 15807565]
45. Sandstrom MC, Johansson E, Edwards K. Influence of Preparation Path on the Formation of Discs and Threadlike Micelles in DSPE-PEG2000/Lipid Systems. Biophys. Chem. 2008; 132:97–103. [PubMed: 18006210]
46. Suloway C, Pulokas J, Fellmann D, Cheng A, Guerra F, Quispe J, Stagg S, Potter CS, Carragher B. Automated Molecular Microscopy: The New Leginon System. J. Struct. Biol. 2005; 151:41–60. [PubMed: 15890530]
47. Hassan PA, Rana S, Verma G. Making Sense of Brownian Motion: Colloid Characterization by Dynamic Light Scattering. Langmuir. 2015; 31:3–12. [PubMed: 25050712]
48. Kleman M, Lavrentovich OD. Liquids with Conics. Liq. Cryst. 2009; 36:1085–1099.
49. Warriner HE, Idziak SHJ, Slack NL, Davidson P, Safinya CR. Lamellar biogels: Fluid-membrane-based hydrogels containing polymer lipids. Science. 1996; 271:969–973. [PubMed: 8584932]
50. Jung HT, Coldren B, Zasadzinski JA, Iampietro DJ, Kaler EW. The Origins of Stability of Spontaneous Vesicles. Proc. Natl. Acad. Sci. U.S.A. 2001; 98:1353–1357. [PubMed: 11171954]
51. Jung HT, Lee SY, Kaler EW, Coldren B, Zasadzinski JA. Gaussian Curvature and the Equilibrium Among Bilayer Cylinders, Spheres and Discs. Proc. Natl. Acad. Sci. U.S.A. 2002; 99:15318–15322. [PubMed: 12444257]
52. van Zanten R, Zasadzinski JA. Using Cryo-Electron Microscopy to Determine Thermodynamic and Elastic Properties of Membranes. Curr. Opin. Colloid Interface Sci. 2005; 10:261–268.
53. Almgren M, Edwards K, Karlsson G. Cryo Transmission Electron Microscopy of Liposomes and Related Structures. Colloids. Surf., A. 2000; 174:3–21.
54. Berstrom LM, Skoglund S, Edwards K, Eriksson J, Grillo I. Self-Assembly in Mixtures of an Anionic and a Cationic Surfactant: A Comparison Between Small-Angle Neutron Scattering and Cryo-Transmission Electron Microscopy. Langmuir. 2013; 29:11834–11848. [PubMed: 23984704]
55. Hunter, RJ. Zeta Potential in Colloid Science: Principles and Applications. San Diego: Academic Press; 1981.
56. Kenworthy AK, Hristova K, Needham D, McIntosh TJ. Range and Magnitude of the Steric Pressure Between Bilayers Containing Phospholipids with Covalently Attached Poly(ethylene glycol). Biophys. J. 1995; 68:1921–1936. [PubMed: 7612834]
57. Kuhl TL, Leckband DE, Lasic DD, Israelchvili JN. Modulation of Interaction Forces Between Bilayers Exposing Short-Chained Ethylene Oxide Headgroups. Biophys. J. 1994; 66:1479–1488. [PubMed: 8061197]

58. Crawford R, Dogdas B, Kerough E, Haas RM, Wepukhulu W, Krotzer S, Burke PA, Sepp-Lorenzino L, Bagchi A, Howell BJ. Analysis of Lipid Nanoparticles by Cryo-EM for Characterizing siRNA Delivery Vehicles. Int. J. Pharm. 2011; 403:237–244. [PubMed: 20974237]

59. Leung AKK, Hafez IM, Baoukina S, Belliveau NM, Zhigaltsev IV, Afshinmanesh E, Tieleman DP, Hansen CL, Hope MJ, Cullis PR. Lipid Nanoparticles Containing siRNA Synthesized by Microfluidic Mixing Exhibit and Electron-Dense Nanostructured Core. J. Phys. Chem. C. 2012; 116:18440–18450.

60. Nakata M, Zanchetta G, Chapman BD, Jones CD, Cross JO, Pindak R, Bellini T, Clark NA. End-to-End Stacking and Liquid Crystal Condensation of 6- to 20- Base Pair DNA Duplexes. Science. 2007; 23:1276–1279. [PubMed: 18033877]

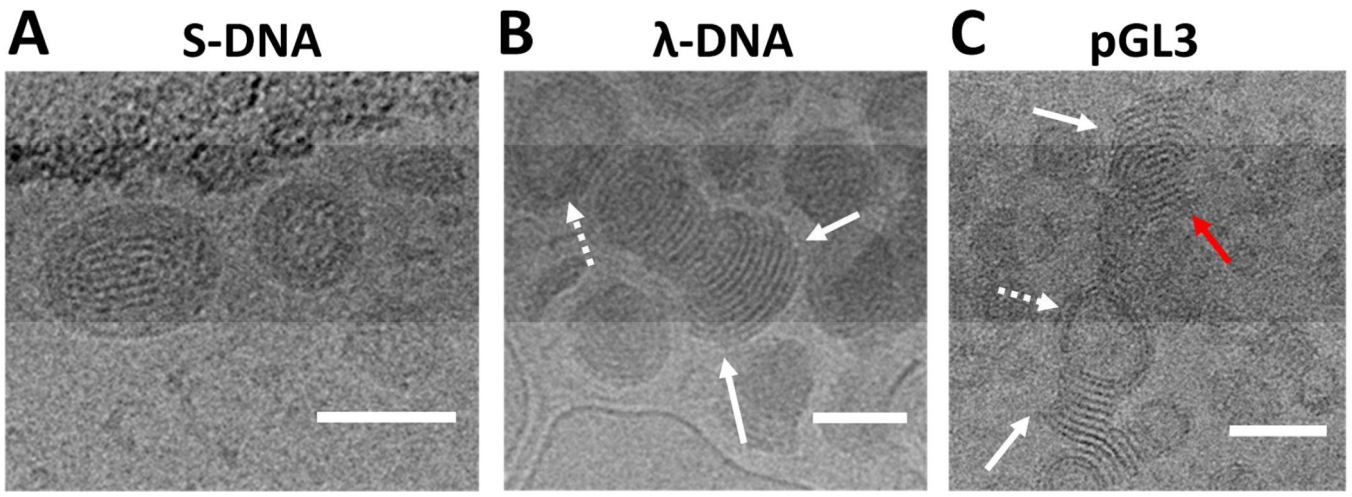

Figure 1.

CL–DNA NPs formed with DNA of different length and topology. (**A**) NPs formed with S-DNA (linear, polydiserse, $L_{mean} \approx 2$ kbps) at a lipid molar ratio of 80/15/5 DOTAP/DOPC/PEG2K-Lipid at $\rho_{chg}= 3$ show a lamellar texture. (**B**) NPs formed with λ-DNA (linear, monodisperse, $L_{mean} \approx 48$ kbps) at lipid ratio of 80/15/5 DOTAP/DOPC/PEG5K–lipid at $\rho_{chg} = 3$ show the lamellar texture as well as terminated bilayer edges (solid arrows). (**C**) NPs formed with pGL3 (circular, monodisperse, $L_{mean} \approx 4.5$ kbps) at a lipid molar ratio of 80/10/10 DOTAP/DOPC/PEG2K-lipid at $\rho_{chg}= 2$ show terminated bilayer edges (solid arrows) similar to (B). In contrast to polydisperse S-DNA, NPs formed with λ-DNA or pGL3 can exhibit hollow cores (dotted arrow) or the lamellar morphology from core to surface (red arrow). All scale bars are 50 nm.

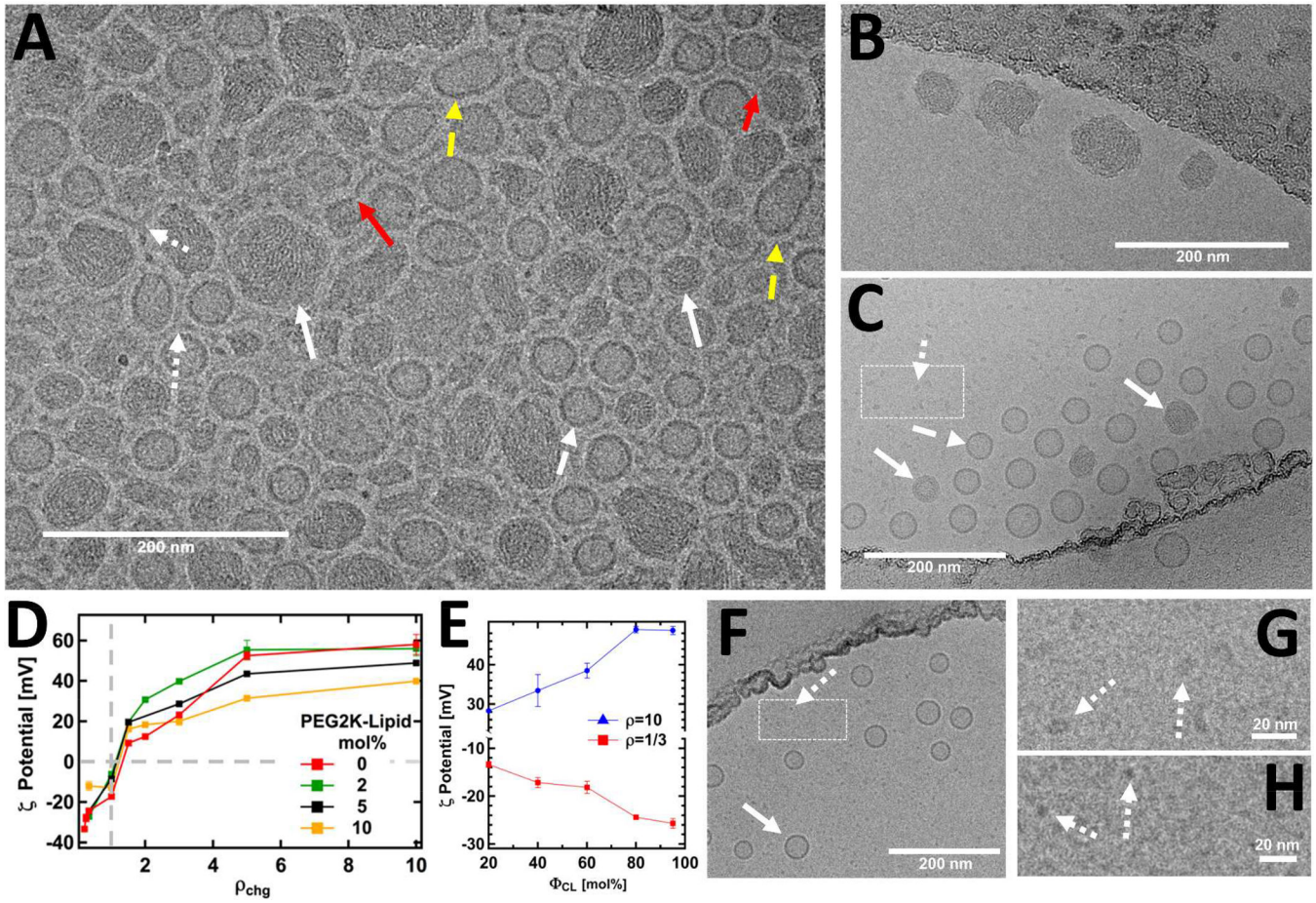

Figure 2.

Overcharged CL–DNA NPs coexist with liposomes and threadlike micelles tor $\rho_{chg} > 1$ (charge molar ratio of cationic lipid to anionic DNA) (**A, B**) Cryo-EM micrograph of CL–DNA NPs formed at a molar ratio of 80/15/5 DOTAP/DOPC/PEG2K-lipid at $\rho_{chg} = 3$ with S-DNA. In (A) the sample was prepared at 30 mg/mL which is the concentration commonly used in small angle x-ray experiments. The sample in (A) was extensively centrifuged to form a pellet, resuspended and imaged, but shows well-defined sub-200 nm NPs. At $\rho_{chg}= 3$, CL–DNA NPs (solid arrows), cationic liposomes (dashed arrows) and small, branched, thread-like micelles (dotted arrows) coexist at equilibrium. Some of the threadlike micelles appear to be protrusions from CL–DNA NPs (red arrows). In (B) the sample was prepared at 3 mg/mL. (**C**) A sample prepared at $\rho_{chg} = 10$ and 3 mg/mL (lipid molar ratio of 80/15/5 DOTAP/DOPC/PEG2K-lipid). The ratio of liposomes (dashed arrows) to CL–DNA NPs (solid arrows) increases with ρ_{chg} as expected. Small spherical micelles are also observed (dotted arrows). (**D**) The zeta potential of CL–DNA NPs at various mol% PEG2K-lipid saturates near $\rho_{chg} \approx 5$. The horizontal and vertical dashed gray lines indicate $\zeta = 0$ mV and $\rho_{chg} = 1$, respectively. (**E**) Plot of the maximum and minimum zeta potential for CL–DNA NPs. This potential strongly depends on the mol% of cationic lipid. (**F**) A control sample containing only liposomes (no DNA). Even at as little as 5 mol% PEG2K-lipid, the unilamellar liposomes (solid arrow) coexist with spherical micelles (dotted arrows). (**G, H**)

Cropped regions (dashed boxes) from C, F). Small sub 5 nm micelles are seen (dotted arrows)Salmon DNA was used in all results shown.

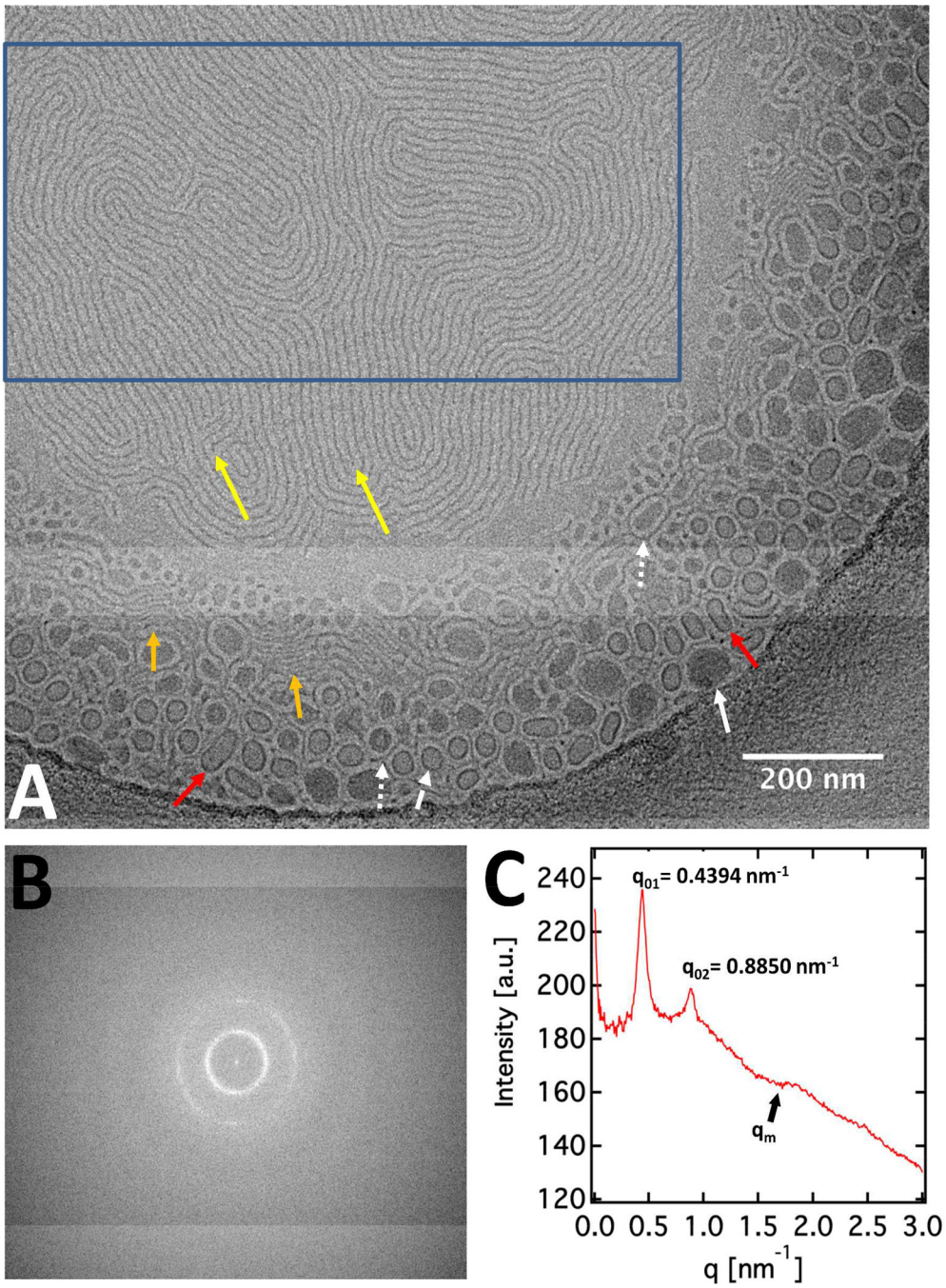

Figure 3.

CL–DNA NPs coexist with threadlike micelles at high concentrations. (**A**) NPs formed at ρ_{chg} = 3 with DOTAP/DOPC/PEG2K-lipid at a molar ratio 80/15/5. with Salmon DNA. Near the edge of the carbon hole, CL–DNA NPs (solid arrow), liposomes (dashed arrow), and micelles (dotted arrows) coexist. The deformed liposomes (red arrows) suggest that the thickness of the suspended water film is comparable to the diameter of the liposomes. This is further substantiated by the spatial organization of all the objects based on size. The center of the water film shows highly ordered thread-like micelles with uniform spacing. The ends

of the thread-like micelles are clearly visible (yellow arrows). Some regions feature what appears to be stacks of 2D ordered micelles (orange arrows). (**B**) A 2D Fourier transform of the boxed region in (A), showing two rings. (**C**) A radial integral of the Fourier Transform in (B) shows two structure factor peaks superimposed on a weak form factor. The peak positions correspond to $q_{on} = n(2\pi/d)$ where d = 14.3 nm (the average spacing between the center of two micelles). The change in slope at $q_m = 1.672\ nm^{-1}$ represents a form factor minimum corresponding to the thickness of the micelles ($\delta_m = 3.727$ nm).

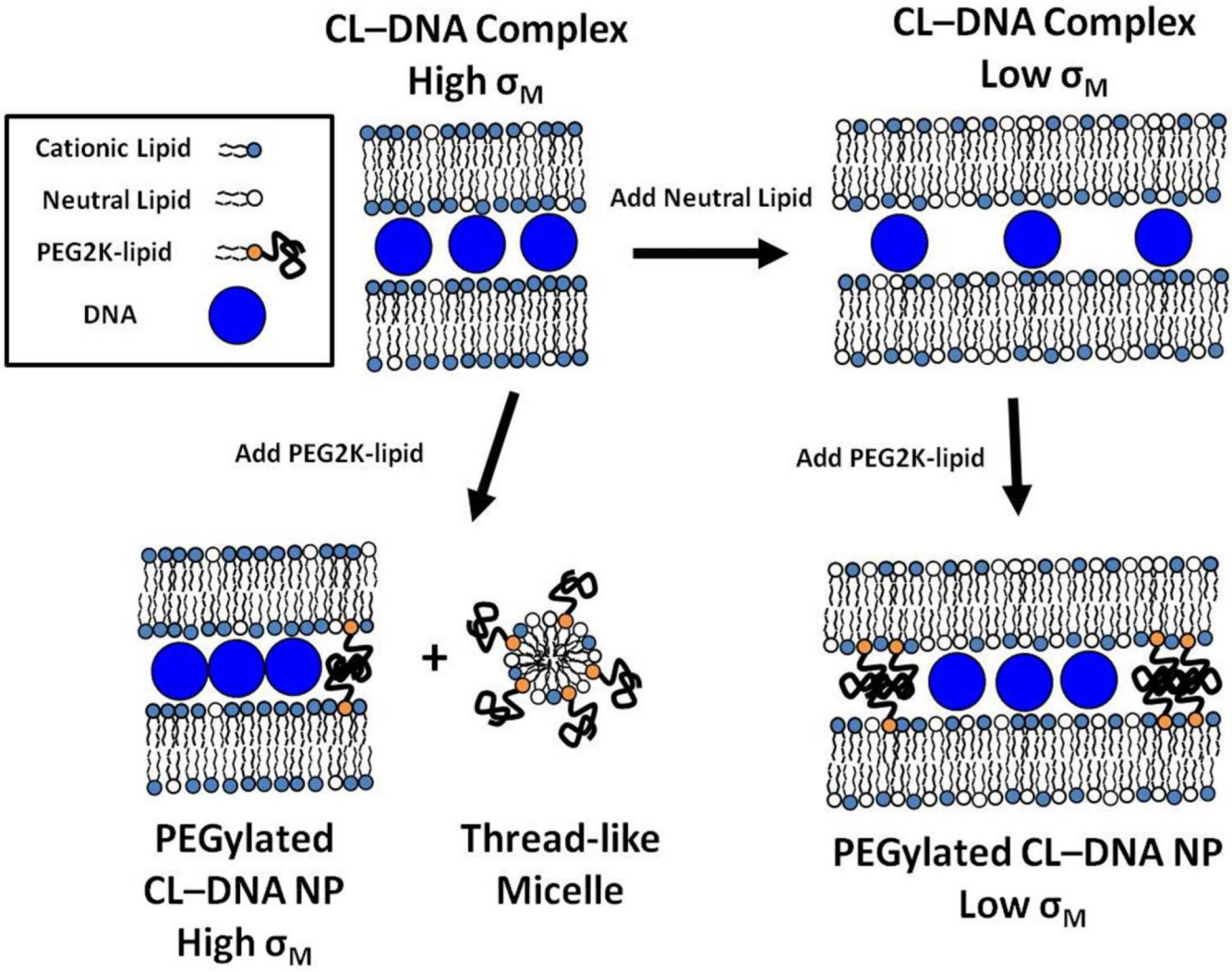

Figure 4.

PEG-lipids and DNA Compete for Available Bilayer Area. Previous work using small angle x-ray scattering (SAXS) shows that DNA spacing in CL–DNA complexes is modulated by neutral lipid content.[16] SAXS has also shown that at low membrane charge density, the addition of PEG-lipid induces a depletion-attraction force which reduces the DNA spacing.[40] We have found that forming high membrane charge density complexes with PEG-lipids results in phase separation of the components into CL–DNA complexes and thread-like micelles because PEG and DNA compete for finite bilayer area.

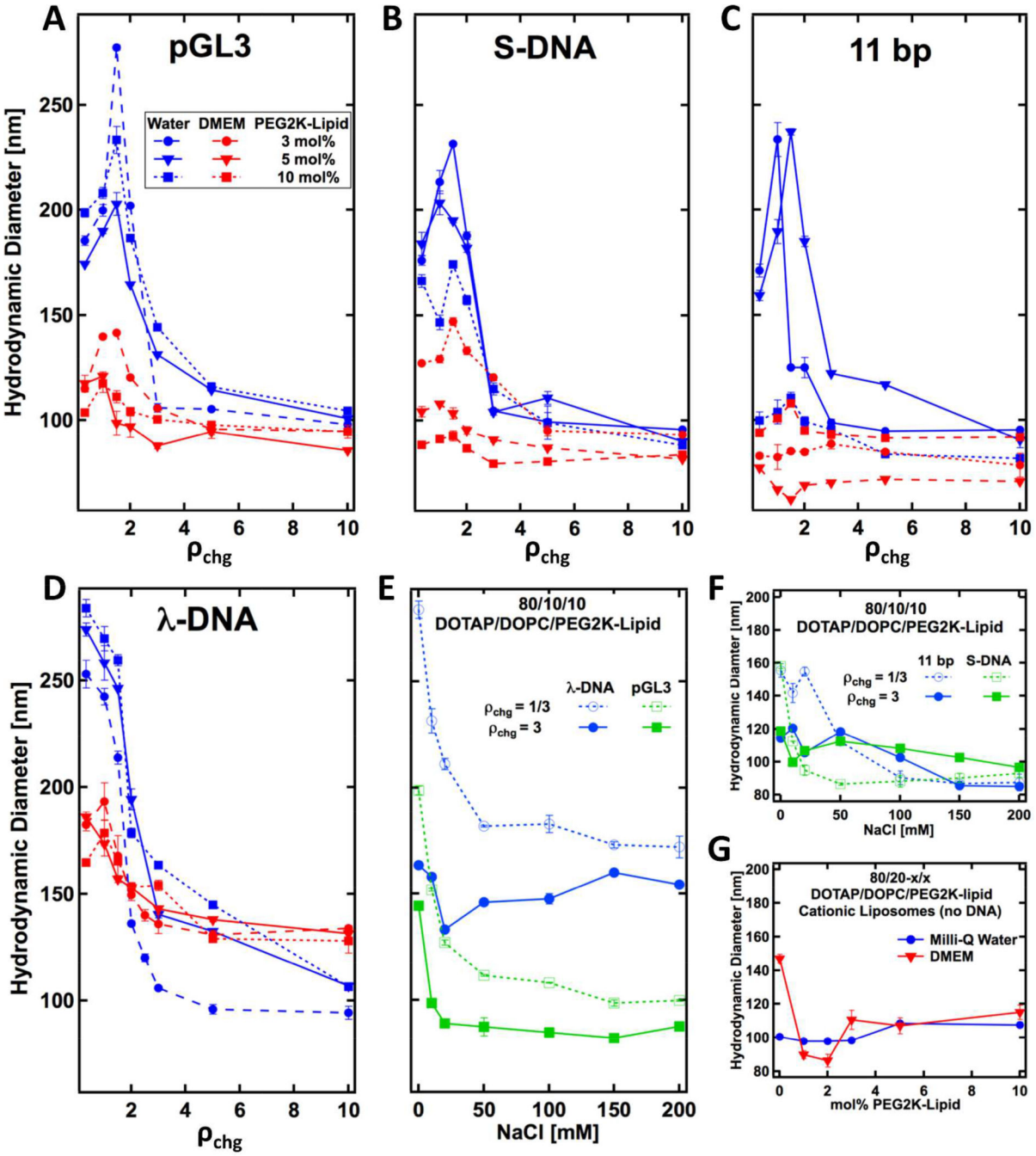

Figure 5.

Measuring CL–DNA NP Size with Dynamic Light Scattering (**A, B, C, D**) Dynamic light scattering results for CL–DNA NPs formed at a lipid molar ratio of 80/20-x/x DOTAP/DOPC/PEG2K-lipid (x = PEG2K-lipid mol fraction) with pGL3(A), S-DNA (B), 11 bp duplex DNA (C), or λ-DNA (D) in either water (blue curves) or DMEM (red curves) as a function of ρ_{chg}. The data in (A), (B) and (C) exhibit a maximum in size near the isoelectric point (ρ_{chg} = 1), while that in (D) shows the diameter continuously increasing as ρ_{chg} decreases below the isoelectric point. The size of NPs not formed with λ-DNA (A, B and C)

tends to be smaller when formed in DMEM. (**E, F**) Hydrodynamic diameter of NPs as a function of ionic buffer strength for λ-DNA (E), pGL3 (E), S-DNA (F) and 11 bp DNA (F). As ionic buffer strength increases, NPs form at smaller sizes. This effect is most pronounced for λ-DNA at $\rho_{chg} = 1/3$ (hollow blue squares in (E)). (**G**) Hydrodynamic diameter of cationic liposomes without DNA in water and DMEM.

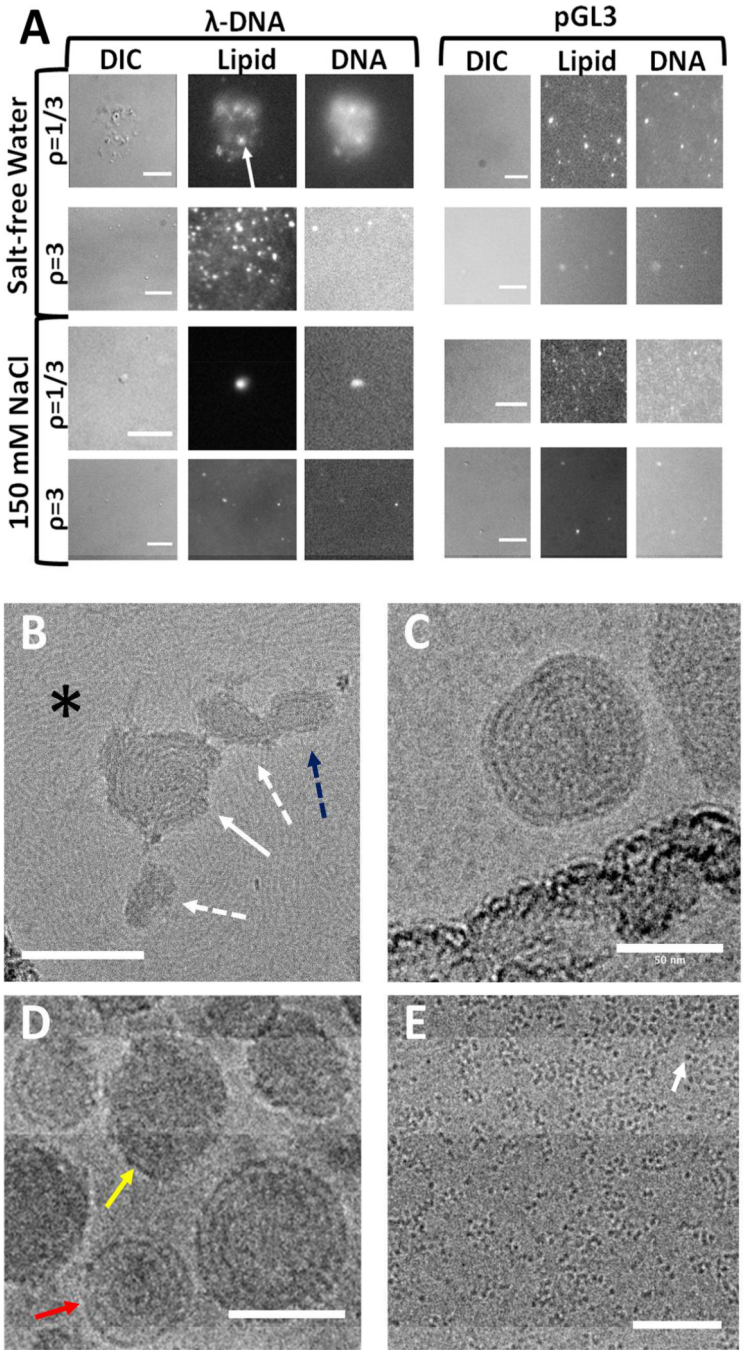

Figure 6.

Fluorescence Microscopy and cryo-EM show that NPs formed at $\rho_{chg}< 1$ with linear DNA can form tethered floes. (**A**) Differential interference contrast (DIC) and fluorescent images (Lipid and DNA) of NPs composed of DOTAP/DOPC/ PEG2K-lipid at a molar ratio of 80/15/5. In nearly all cases, small diffraction-limited spots show colocalization of the lipid and DNA signal. The exception is λ-DNA NPs at $\rho_{chg}= 1/3$ formed in water, where discrete NPs are visible in the lipid channel while the DNA channel shows condensed fluorescent spots surrounded by a fuzzy cloud. The cloud of DNA is due to the presence of loose DNA

tethering the NPs. All scale bars are 5 μM. (**B, C**) NPs formed with 80/15/5 molar ratio of DOTAP/DOPC/ PEG2K-lipid with S-DNA at ρ_{chg} = 1/3 (B) and ρ_{chg} = 3(C). In (B) an NP with onion-like morphology is tethered to two smaller NPs (dashed arrows). At ρ_{chg}< 1, NPs coexist with excess DNA in solution (asterisk). (**C**) An onionlike NP at ρ_{chg} > 1 with no excess DNA in the background. (**D, E**) Cryo-EM micrographs of a solution containing 80/10/10 DOTAP/DOPC/PEG2K-lipid NPs formed with 11 bp DNA at ρ_{chg} = 1/3. In (D) two NP morphologies are observed; onions with condensed bilayers (red arrow) and featureless, electron-dense globules (yellow arrow). (E) shows the excess 11 bp DNA in solution. All cryo-EM scale bars are 50 nm.